Applied Surface Science Advances 31 (2026) 100916

Contents lists available at ScienceDirect

Applied Surface Science Advances

journal homepage: www.sciencedirect.com/journal/applied-surface-science-advances

Full Length Article

Defect analysis of Al-delta-doped ZnO thin films by positron annihilation spectroscopy

Guoxiu Zhang [a,b], Maciej Oskar Liedke [c], Maik Butterling [d], Eric Hirschmann [c], Andreas Wagner [c], René Hübner [a], Shengqiang Zhou [a], Manfred Helm [a,e], Elizabeth von Hauff [b,f], Slawomir Prucnal [a,*]

[a] Helmholtz-Zentrum Dresden-Rossendorf, Institute of Ion Beam Physics and Materials Research, Bautzner Landstrasse 400, Dresden 01328, Germany
[b] Faculty of Electrical and Computer Engineering, TU Dresden, Dresden 01069, Germany
[c] Helmholtz-Zentrum Dresden-Rossendorf, Institute of Radiation Physics, Bautzner Landstrasse 400, Dresden 01328, Germany
[d] Reactor Institute Delft, Department of Radiation Science and Technology, Faculty of Applied Sciences, Delft University of Technology, Mekelweg 15, NL-2629 JB Delft, Netherlands
[e] Faculty of physics, TU Dresden, Dresden 01069, Germany
[f] Fraunhofer Institute for Electron Beam and Plasma Technology FEP, Dresden 01277, Germany

ARTICLE INFO

Keywords:
Positron annihilation
Delta-doping
Zinc oxide (ZnO)
Defect analysis
Atomic layer deposition (ALD)
Flash-lamp annealing (FLA)

ABSTRACT

Zinc oxide (ZnO) is a wide-bandgap semiconductor with excellent optical and electrical properties, making it a promising material for a wide range of applications in optoelectronics and sensors. The properties of ZnO can be easily modified through doping and defect engineering, which determines its long-term stability and ultimate application. One of the most well-known dopants for ZnO is aluminum (Al), which is used to produce the transparent conductive oxide AZO. In this study, using positron annihilation spectroscopy (PAS) and photoluminescence (PL), we demonstrate defect engineering in AZO through millisecond flash-lamp annealing. We show that the nature of the defects strongly depends on the Al-concentration. The highest electrical conductivity of AZO is obtained at an Al:Zn layer ratio of 1:20, i.e., 2.64 at. % Al. Samples with higher Al content are more resistant to annealing and contain more defects. PAS results reveal the presence of zinc vacancies (V_{Zn}) and zinc–oxygen vacancy complexes (V_{Zn+O}) in the delta-AZO thin films, and although the PAS and PL results are generally consistent, slight differences suggest the possible existence of non-optically active defects that are not revealed by the PL measurements. Additionally, an appropriate amount of aluminum doping contributes to improving the crystallinity of ZnO.

1. Introduction

Wide-bandgap semiconductors, i.e., with a bandgap typically larger than 2.3 eV, have gained considerable interest in recent years due to their exceptional electrical, optical, and thermal properties [1,2]. These materials are particularly attractive for high-performance applications in optoelectronics and power electronics, where conventional semiconductors are no longer able to meet the increasing demands of high-frequency, high-temperature, and high-power devices. The large energy gap of these semiconductors offers advantages such as high breakdown voltage, low leakage current, and excellent thermal stability, making them ideal for use in devices such as high-power transistors, UV emitters, and transparent conductive films [3,4]. However, the synthesis and doping processes of wide bandgap materials present several technical challenges, particularly in terms of high-quality crystal growth, precise defect control, and doping uniformity. These challenges can have a direct impact on the material's electrical properties, stability, and overall suitability for practical applications. In particular, wide-bandgap semiconductors exhibit asymmetric doping properties due to their energetically high conduction band minimum (CBM) and energetically low valence band maximum (VBM) [5]. Achieving p-type doping is particularly challenging because acceptor levels are typically located energetically far from VBM, making hole activation difficult. Although wide bandgap materials show n-type conductivity due to intrinsic defects, achieving high electron concentration remains a challenge because acceptors, such as cation vacancies, compensate for the doping

* Corresponding author.
E-mail address: s.prucnal@hzdr.de (S. Prucnal).

https://doi.org/10.1016/j.apsadv.2025.100916
Received 25 September 2025; Received in revised form 3 December 2025; Accepted 3 December 2025
Available online 9 December 2025

effect of donor impurities.

Zinc oxide (ZnO), with a direct bandgap of approximately 3.37 eV at 300 K, has attracted considerable interest due to its excellent optical and electrical properties, as well as its low fabrication costs. Thin ZnO films have promising applications in optoelectronics, sensors, transparent conductive electrodes, low-emissivity coatings, and catalysts [6–9]. Typically, ZnO films exhibit a background electron concentration in the range of 10^{15} to 10^{19} cm^{-3}, which is due to defects such as zinc interstitials (Zn_i) and oxygen vacancies (V_O). Doping ZnO with group-III elements like aluminum (Al) or gallium (Ga) can significantly increase the electron concentration, reaching values between 10^{20} and 10^{21} cm^{-3}, thereby improving conductivity and making it a key candidate for use in transparent conductive layers and infrared reflectors [8,10].

Post-deposition thermal processing is a critical determinant of the electronic properties. Our prior study on delta-doped ZnO confirmed that flash-lamp annealing (FLA) successfully improved the electrical conductivity by efficiently activating dopants while suppressing unwanted diffusion of the dopants [11]. In contrast, rapid thermal annealing (RTA) or furnace annealing causes Al diffusion, resulting in the formation of non-conductive aluminum oxide, thereby decreasing the conductivity of Al-doped ZnO films [11]. The key advantage of FLA compared to other conventional annealing techniques rely on: (i) defect engineering and dopant activation without dopant diffusion [12], (ii) the presence of a temperature gradient along the sample cross-section that allows annealing of thin films on temperature-sensitive substrates like ITO on polymer or glass [13], (iii) lower costs due to more efficient energy managing [14].

In our previous work, we fabricated Al-delta-doped ZnO thin films with improved electrical and optical properties using atomic layer deposition (ALD) and FLA [11]. By optimizing the annealing conditions as well as varying the thickness of undoped ZnO and the Al-concentration, we achieved carrier concentration as high as 2.7×10^{21} cm^{-3}, over 80 % transparency in the visible range, and excellent infrared reflectivity [11]. However, the electrical properties of thin ZnO layers are influenced by various factors related to their structure. Understanding the process of defect formation during ultra-short annealing and the influence of sample preparation on the type of defects formed in the layer is critical for the performance of the fabricated layers.

In the current work, we used positron annihilation lifetime spectroscopy (PALS) and Doppler-broadening variable-energy positron annihilation spectroscopy (DB-VEPAS) in combination with X-ray diffraction and photoluminescence spectroscopy to identify the type of defects and shed light on how defects can be controlled and utilized. PALS is a highly sensitive technique, ideal for analyzing open-volume defects in Al-delta-doped ZnO films such as single [15] and multiple zinc vacancies [16]. DB-VEPAS allows us to gain detailed information on the types and distributions of defects, which are crucial for understanding the improved electrical properties of the layer [17,18]. Furthermore, PALS reveals the size of the positron traps, as the positron annihilation time increases with the defect size. Through the integrated analysis with these techniques, we were able to better understand the relationship between defects and the electrical performance of thin Al-delta-doped ZnO layers.

2. Experiments

2.1. Sample preparation

Thin ZnO and AZO layers were deposited on a Si-substrate at 200 °C using the atomic layer deposition (ALD). Details on sample preparation can be found in our previous work [11]. As shown in Table 1, each AZO thin film varies with an Al:Zn layer ratio of 1:40, 1:30, 1:25,1:20, 1:10, and 1:5 and has a thickness of approximately 100 nm and Al-concentrations of 0.24, 0.96, 1.27, 2.64, 5.32, and 12.5 at. %, accordingly. When assigning sample numbers to individual thin layers, we use different capital letters to distinguish between different Al contents in the ZnO layers. The layers were annealed independently by flash-lamp annealing in a nitrogen atmosphere for 23 ms at a flash energy density of 66.4 J/cm^2 or 109.7 J/cm^2. The samples labeled with a capital letter and "0" correspond to layers without annealing, the samples labeled with "1" were annealed at 66.4 J/cm^2, and the samples labeled with "2" were annealed at 109.7 J/cm^2. Note that due to its ultra-short heating and cooling time, FLA was also used to process AZO films grown on flexible polymer substrates [19].

Table 1
Sample number, sample name, Al:Zn layer ratio, Al-concentration, and the post-growth treatment applied to the fabricated layers.

Sample No.	Sample name	Al:Zn layer ratio	Al concentration (at. %)	Flash energy density (J/cm^2)
A0	As-deposited ZnO	-	0	-
A1	Flashed ZnO	-	0	66.4
A2	Flashed ZnO	-	0	109.7
B1	Flashed AZO	1:40	0.24	66.4
C1	Flashed AZO	1:30	0.96	66.4
D1	Flashed AZO	1:25	1.27	66.4
E0	As-deposited AZO	1:20	2.64	-
E1	Flashed AZO	1:20	2.64	66.4
E2	Flashed AZO	1:20	2.64	109.7
F1	Flashed AZO	1:10	5.32	66.4
G0	As-deposited AZO	1:5	12.5	-
G1	Flashed AZO	1:5	12.5	66.4

The microstructural properties of the fabricated films were investigated by X-ray diffraction (XRD) and cross-sectional transmission electron microscopy (TEM). An X-ray diffractometer (Rigaku SmartLab) with a Cu-Kα source and Bragg-Brentano geometry was used to investigate the structural properties. The θ/2θ scans were performed for diffraction angles ranging from 20° to 60°. Cross-sectional high-angle annular dark-field (HAADF) scanning transmission electron microscopy (STEM) was performed with an FEI Talos F200X microscope to see the microstructure of the ZnO and AZO thin layers deposited on Si wafers. The room-temperature PL measurements were used to determine the optical properties of the as-grown and annealed samples. The ZnO and AZO layers were optically excited by a Xe-lamp at the wavelengths of 260 nm, and the signal was recorded with an iHR550 spectrometer and a photomultiplier, Hamamatsu H7732–10.

2.2. Doppler-Broadening variable-energy positron annihilation spectroscopy (DB-VEPAS)

Doppler-broadening variable-energy positron annihilation spectroscopy (DB-VEPAS) measurements were conducted at the apparatus for *in-situ* defect analysis (AIDA) [20] of the slow positron beamline (SPONSOR) [21]. Positrons were accelerated and mono-energetically implanted into the samples in the range between E_p = 0.05–7.5 keV. The various E_p allows for depth profiling. A mean positron implantation depth ($\langle z \rangle$) was approximated using the material density (ρ) dependent formula [22]:

$$\langle z \rangle = \frac{36}{\rho} E_p^{1.62} \quad (1)$$

$\langle z \rangle$ is expressed in nm, ρ is given in g/cm^3, and E_p is in keV, $\langle z \rangle$ approximates the depth as it does not account for positron diffusion. When implanted into a solid, positrons lose their kinetic energy through thermalization, and after short diffusion, annihilate either at delocalized lattice sites (bulk annihilation) or within vacancy-like defects and interfaces. Upon annihilation with electrons, they typically emit two anti-collinear 511-keV gamma photons. Since thermalized positrons have minimal momentum compared to electrons at the annihilation site, a broadening of the 511-keV line is observed, primarily due to the

momentum of the electrons. This broadening here is measured using high-purity Ge detectors, with an energy resolution of 1.09 ± 0.01 keV or 0.78 ± 0.02 keV at 511 keV for single-detector and double-detector configurations, respectively. The broadening is characterized by two distinct parameters, S and W, which correspond to the fraction of the annihilation line in the central (511 ± 0.93 keV) and outer (508.33 ± 0.49 keV and 513.67 ± 0.49 keV) regions, respectively. The S-parameter is a fraction of positrons annihilating with low momentum valence electrons and represents vacancy-type defects and their concentration. The W-parameter approximates the overlap of the positron wave-function with high-momentum core electrons. Plotting the calculated S as a function of positron implantation energy, $S(E_p)$, provides depth-dependent information, whereas S-W plots are used to examine the atomic surroundings of the defect site and its size (type) [23].

Coincidence Doppler broadening (cDB) measurements of the annihilation peak , where both annihilation photons are recorded at the same time, is sensitive to atomic decoration of the defect site. Every chemical element has a unique shape of the cDB spectrum. The effective momentum of an annihilating electron-positron pair consists mostly of the electron momentum. The measured Doppler shift in the energy of the annihilation photons yields the momentum distribution of electrons that have annihilated positrons. In addition, a huge advantage of that method is that the accidental events from the background are not recorded, which improves the signal-to-noise ratio. The difference in energies of the two annihilation photons is $E_1 - E_2 = 2 \cdot \Delta E = c \cdot p_L$, where c is the speed of light and p_L is the longitudinal component of the electron momentum in the direction of the emitted annihilation photon [24].

2.3. Variable-Energy positron annihilation lifetime spectroscopy (VE-PALS)

Variable-energy positron annihilation lifetime spectroscopy (VE-PALS) measurements in the implantation energy E_p range of 0.5 - 7.5 keV were conducted at the Mono-energetic Positron Source (MePS) beamline, which is an end station of the radiation source ELBE (Electron Linac for beams with high Brilliance and low Emittance) at Helmholtz-Zentrum Dresden-Rossendorf (HZDR), Germany [17]. A $CeBr_3$ scintillator detector coupled to a Hamamatsu R13089–100 photomultiplier (PMT) tube was utilized for gamma quanta acquisition, and the signals were processed by the SPDevices ADQ14DC-2X digitizer (14 bits vertical resolution and 2GS/s horizontal resolution) [25]. The overall time resolution of the measurement system is ≈0.250 ns, and all spectra contained at least 1×10^7 counts. A typical lifetime spectrum $N(t)$, the absolute value of the time derivative of the positron decay spectrum, is described by

$$N(t) = R(t) * \sum_{i=1}^{k+1} \frac{I_i}{\tau_i} e^{\frac{-t}{\tau_i}} + \text{Background} \quad (2)$$

where k is the number of different defect types contributing to the positron trapping, which are related to $k+1$ components in the spectra with the individual lifetimes τ_i and intensities I_i (ΣI_i=1) [26]. The instrument resolution function $R(t)$ is a sum of two Gaussian functions with distinct intensities and relative shifts, both depending on the positron implantation energy, E_p. It was determined by the measurement and analysis of a reference sample, i.e., Yttria-stabilized zirconia (YSZ), which exhibited a single well-known lifetime component. The background was negligible, since close to zero.

All the spectra were deconvoluted using a non-linear least-squares fitting method, minimized by the Levenberg-Marquardt algorithm, employed within the fitting software package PALSfit [27] into 3 discrete lifetime components, which directly evidence localized annihilation at two different defect types (sizes; τ_1 and τ_2). The third component τ_3 is necessary for the fit but negligible (I_3<1 %). Relative intensities reflect the concentration of each type of defect (size). In general, the positron lifetime is directly proportional to defect size, i.e., the larger the open volume, the longer the lifetime [26,28]. The positron lifetime and its intensity were probed as a function of the positron implantation energy (E_p), or equivalently, the positron implantation depth $\langle z \rangle$. The average positron lifetime τ_{av} is defined as $\tau_{av} = \sum_i \tau_i \cdot I_i$ and is strongly affected by the defect type (size).

3. Results and discussion

3.1. Structural characterization

The investigated AZO layers were deposited on the Si substrates at 200 °C by ALD. Due to the high deposition temperature, the as-deposited layers exhibit a certain degree of order and initial crystallization. Typically, ZnO deposited on various substrates shows columnar growth, but the crystallinity strongly depends on the substrate and growth temperature [29]. The main diffraction peaks observed here from the as-deposited ZnO and AZO (1:20) samples are located at about 31.89° and 34.53° (see Fig. 1a). Moreover, a weak peak at about 36.28° is distinguishable. These three peaks are assigned to the (100), (002), and (101) planes of ZnO, where their position according to the JCPDS file No. 00–036–1451 should be at 31.769°, 34.421°, and 36.252°, respectively. The slight shift of all peaks towards bigger angles suggests compressive strain that is stronger along (002) plane than along (100) plane. The sample AZO (1:10) shows well-resolved three peaks. The reflection from (101) plane is much stronger than from the other samples. It suggests that more Al incorporated into the ZnO matrix causes stronger disorder and suppresses the formation of textured film as the former shows no (101) reflection. Moreover, the main reflections from (100) and (002) planes are shifted to even larger angles, suggesting the strong reduction of the lattice parameter in the fabricated AZO film [30,31]. The sample grown with an Al:Zn layer ratio of 1:5 presents only broad weak peaks at about 32.67° and 36.20°, which is typical for amorphous or strongly disordered systems.

Fig. 1b) shows the XRD patterns obtained from the samples annealed by FLA for 23 ms at an energy density of 109.7 J/cm^2. In the case of undoped ZnO, the diffracted intensity increases fourfold and the 002 peak position shifts by 0.1° from 34.43° to 34.55° This suggests a significant improvement in the layer crystallinity upon FLA. Samples containing a small amount of Al (Al:Zn layer ratio of 1:20, 2.64 at. %) revealed good crystallinity already in the as-deposited state according to Fig. 1a). After FLA, the peak intensity has increased slightly, but the peak position shifts by 0.1° towards larger angles. For AZO 1:10, flash lamp annealing (FLA) increased the intensities of all peaks. However, with further increase in Al content, FLA no longer had a noticeable effect, and the XRD peak intensities remained unchanged.

In order to investigate the change in crystallinity of the Al-doped ZnO as a result of FLA treatment, we performed high-resolution scanning transmission electron microscopy imaging of the AZO layers with an Al:Zn layer ratio of 1:20.

Importantly, the samples show planar growth of the Al-doped layers and the quantum-well structure is preserved until the end of the growth process. As marked in Figs. 2b) and d), the pure ZnO and Al-containing $AlZnO_x$ layers can be easily distinguished, and the layer-by-layer structure is maintained after annealing. In the case of the sample having an Al:Zn layer ratio of 1:20, the average distance between the Al layers is about 2.5 nm, which agrees well with the thickness predicted based on the growth rate of AZO in our ALD system.

3.2. Photoluminescence spectroscopy of fabricated films

Fig. 3 shows the room temperature PL spectra obtained from undoped and Al-doped ZnO films in the as-deposited stage and after annealing. Samples were excited using a 260 nm light source, which corresponds to an average penetration depth of approximately 50 nm, about half the layer thickness. Fig. 3a) shows the PL spectra obtained from undoped ZnO. The as-deposited sample exhibits weak near

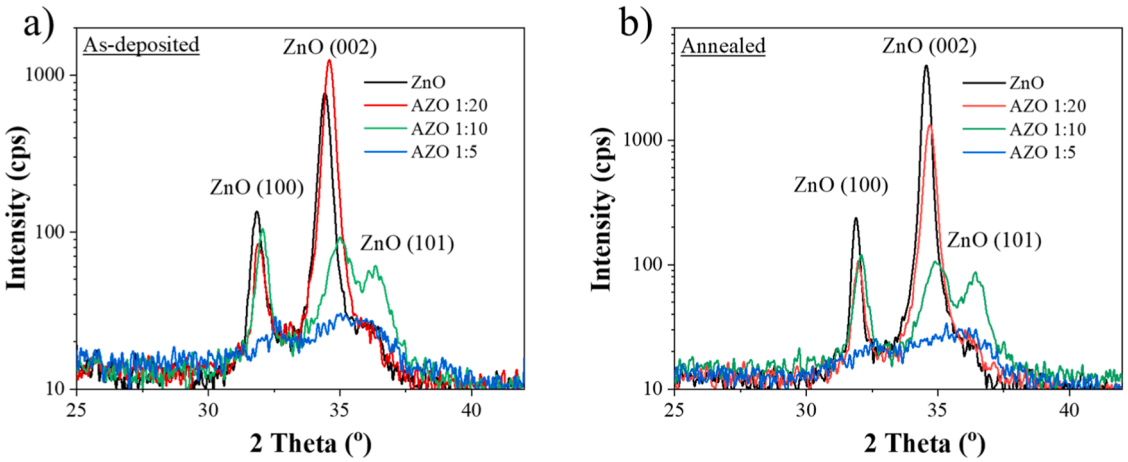

Fig. 1. X-ray diffraction patterns of as-deposited (a) and flash-lamp annealed samples (b) grown on Si substrates by ALD. The samples were annealed for 23 ms at an energy density of 109.7 J/cm^2.

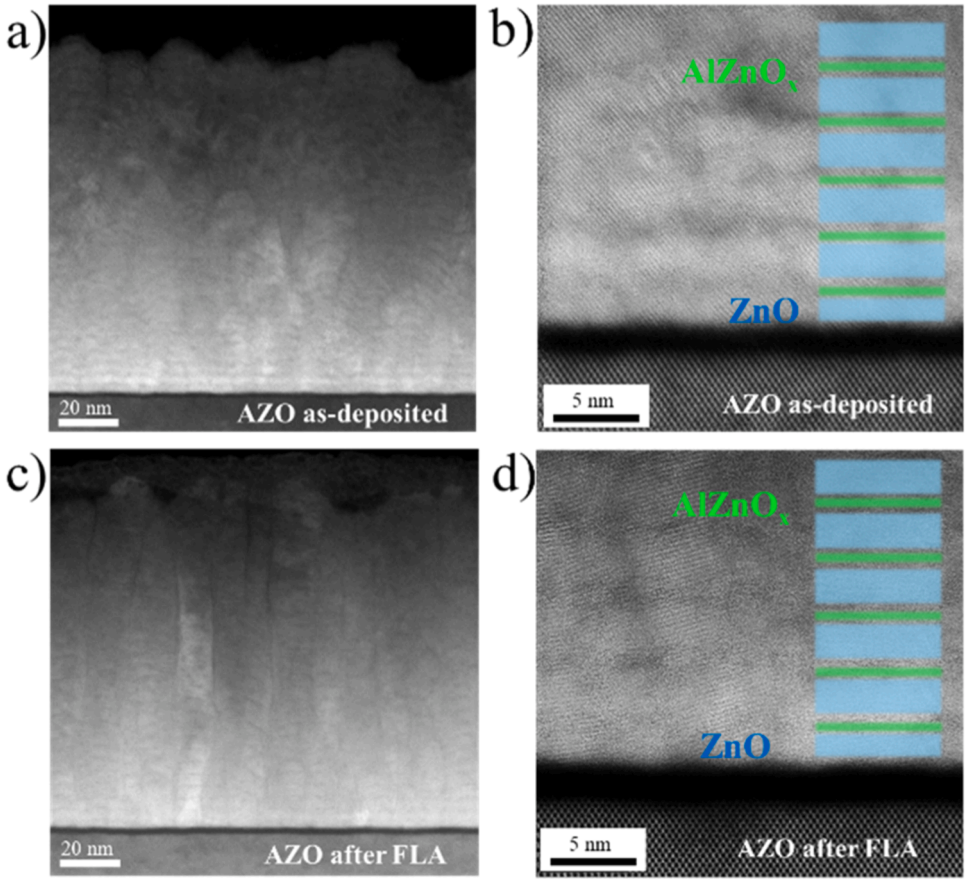

Fig. 2. Overview (a, c) and high-resolution STEM images close to the Si substrate (b, d) of the as-deposited AZO (1:20) films (a, b) and after flash-lamp annealing (c, d). FLA was performed for 23 ms at an energy density of 109.7 J/cm^2. The blue and green regions in panels b and d schematically show the thicknesses of the undoped ZnO and Al-doped ZnO layers.

bandgap emission (NBE) at about 375 nm and a red-emission at about 650 nm from a donor-acceptor pair (DAP). In undoped ZnO, the DAP is related to the deep-acceptor level due to interstitial [32]. After FLA, the NBE increases significantly, and the DAP emission shifts to the green spectral range. The main emission is at about 520 nm and typically is assigned to the zinc-vacancies (V_{Zn}) or oxygen-vacancies (V_O) [33,34]. Since our samples are grown in oxygen-rich conditions, the green luminescence can be caused by zinc vacancies. A strong enhancement of the NBE after FLA confirms an improvement in the crystal quality of the grown layers. The higher carrier concentration of flashed AZO (1:20) compared with ZnO leads to a blueshift of the NBE emission, which arises from the Burstein-Moss effect due to conduction band filling [11]. Meanwhile, in annealed AZO 1:20, defect-related emissions are barely observed, in contrast to pure ZnO, where pronounced green emission appears after annealing. This difference can be attributed to successful Al incorporation, which stabilizes the ZnO lattices, and reduced

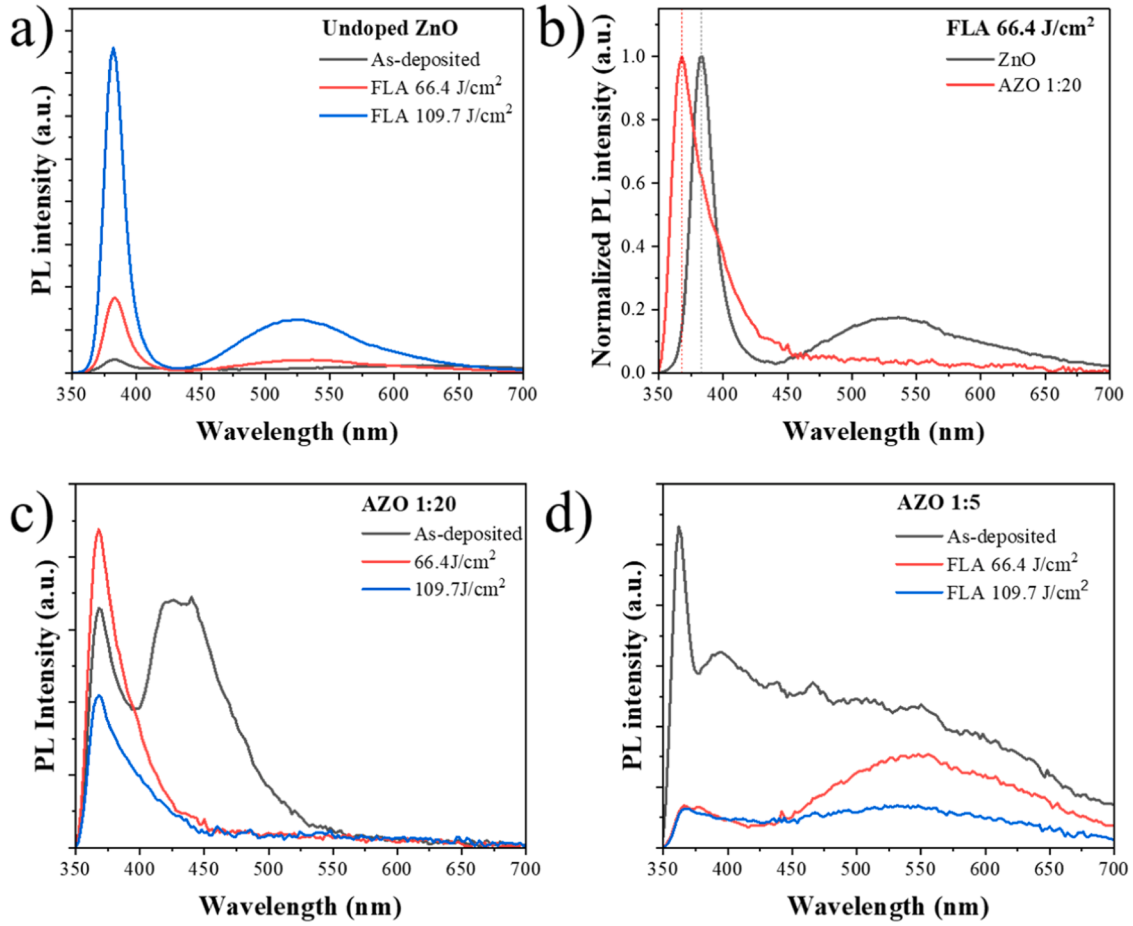

Fig. 3. Room temperature PL spectra after excitation with Xe-lamps at the 260 nm wavelength of ZnO and AZO before and after flash lamp annealing under N_2 for 23 ms with different energy densities.

defect-related emissions.

3.3. Defect characterization by positron annihilation spectroscopies

Positron annihilation spectroscopy is one of the most sensitive techniques to investigate negatively charged and neutral point defects in solids. The interaction of positrons with solids and their lifetime depend on the defect density and type of defects. Typical positron lifetime, i.e., the time counted from the incident of the positron with the solid and emission of the gamma-photons with an energy of about 511 keV, is in the order of several tens to hundreds of ps, for bulk and annihilation at vacancy agglomerations. Variable-Energy Positron Annihilation Lifetime Spectroscopy (VEPALS) allows to determine the type (size) of defects like mono- or multivacancy, their concentration, and depth distribution. On the other hand, Doppler-broadening Variable-Energy Positron Annihilation Spectroscopy (DB-VEPAS) provides more general information about open volume defects evolution, including concentration and the depth distribution determined from the change of the value of S-parameter, and about the chemical environment of defects determined from the W-parameter.

3.3.1. Doppler broadening variable energy positron annihilation spectroscopy

First, we used DB-VEPAS measurements to determine the defect concentration variation in as-grown samples and the influence of the post-grown FLA on the evolution of the defects. Fig. 4a) shows the change of the S and W-parameter as a function of the layer thickness for as-deposited ZnO and Al-doped ZnO films with an Al:Zn layer ratio of 1:20. The most defective regions of any solids are typically located at the surface and often interfaces between layers. The larger S-parameter from the surface region corresponding to the positron energy implantation of ~1 keV indicates increased defect density. In the bulk of the film, with positron implantation energy between 2 and 4 keV, the S-parameter has the lowest value ~0.54. For higher positron implantation energies, the value of the S-parameter increases due to the transition to the Si-substrate having a much larger intrinsic S-parameter. In the case of the W-parameter, the distribution of values resembles the inverted distribution of the S-parameter. The W-parameter describes positrons annihilating with a core electron (inner-shell electron), as a result, the emitted gamma-ray has slightly higher energy and can be found in the "wings" of the Doppler broadening spectrum. In general, the as-deposited samples with Al have a larger S-parameter than undoped ZnO, indicating an increased concentration of Al convoluted with slightly larger defect density. This result can be attributed to the doping effect (annihilation of positrons with electrons in the volume of the Al-doped ZnO film) and point defects.

Fig. 4b compares the S- and W-parameters of undoped ZnO film and AZO films with different Al-concentrations flashed with an energy density of 66.4 J/cm^2. When the Al-to-Zn layer ratio is smaller than 1:20, meaning low Al concentration in the sample, the S parameter is the lowest, even lower or comparable with the undoped ZnO film. It suggests the increased Al-content; however, the overall vacancy defect density remains similar, as the curve slope below 2–3 keV is quite the same. That slope represents positron back-diffusion to the surface, which is related to the number of traps they eventually encounter. Still, small variations in the concentration of open volume defects like Zn-vacancies are possible. On the other hand, when the layer ratio is 1:5, corresponding to the highest Al doping concentration, the S parameter is the

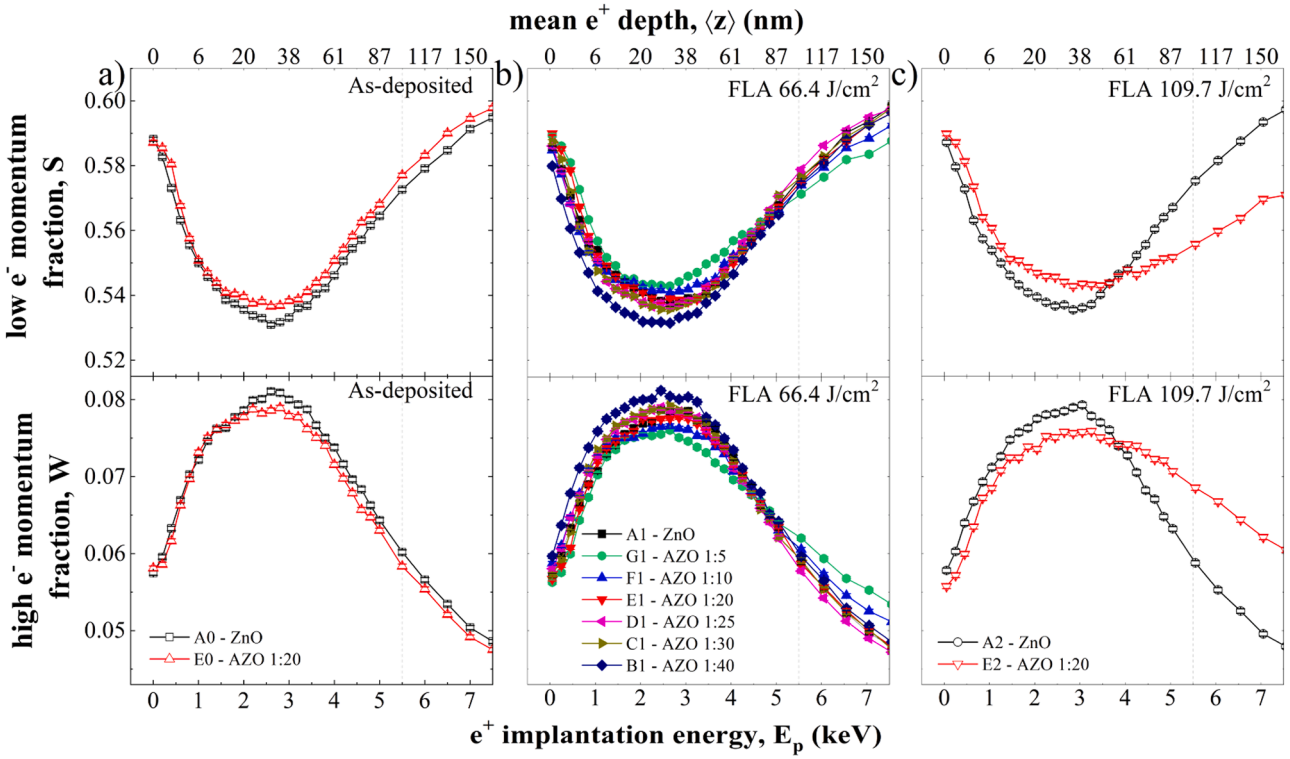

Fig. 4. S and W parameters as a function of incident positron energy (E_p) of 100-nm thick layers (a) as-deposited ZnO and AZO having an Al:Zn layer ratio of 1:20, b) ZnO and AZO films having Al:Zn layer ratios of 1: X (X = 40, 30, 25, 20, 10, and 5) treated by FLA with a flash energy density of 66.4 J/cm^2, and c) ZnO and AZO having an Al:Zn layer ratio of 1:20 treated with a flash energy density of 109.7 J/cm^2. The interfaces between ZnO or AZO thin films and substrates are shown as the dashed lines.

highest, reflecting the largest defect density. This suggests that a moderate amount of Al doping likely facilitates the repair of the ZnO lattice. Next, looking at Fig. 4c) and comparing it with the data presented in Fig. 4a), we can see that after further increasing the annealing energy density (annealing temperature), the S parameter increases, i.e., the average volume of positron annihilation centers also increases. Hence, we can conclude that the increase of S-parameter after annealing at 109.7 J/cm^2 is a consequence of raising open volumes in ZnO, but a higher layer conductivity could play an additional role. The detailed studies of the influence of the annealing and doping parameters on the layer conductivity can be found in Ref [11].

Fig. 5a) presents the plot of the S-parameter as a function of W-parameter collected from flashed ZnO and AZO films containing different Al-concentration. The S and W parameters were estimated at a depth of about 31 nm, which corresponds to the positron implantation energy of 2.65 keV. Two extreme points are from single crystal ZnO (marked in blue) and from bulk aluminum (marked with magenta). The measurement points are located between both references along a line indicating the existence of a similar type of defect. In order to gain more details about defects, Fig. 5b) shows an enlarged part of S-W points reflecting the experimental results only. The closest point to the bulk defect-free ZnO is S-W value obtained for the sample with Al:Zn ratio of 1:40. Next, with increasing Al-concentration, the S-W value moves towards the bulk Al. The shift in direction of Al defect-free reference visualizes the rising Al decoration of the annihilation site, at the vacancy-like defects, and superimposed increase of defect density, as the S-parameter rises. Interestingly, undoped ZnO is located between 1:20 and 1:25. This suggests that a small amount of Al could improve the ZnO crystallinity, while a high doping level increases the defect concentration. However, we cannot exclude that the absolute values of S-W are not dominated by counterparts related to the chemical differences of both films, superimposed in addition with contributions from open volumes. On the other hand, we have shown previously that increasing decoration of zinc-oxygen vacancy complexes that dominate the defect landscape in our AZO films, as will be shown based on PALS later, with Al does not change the electron momentum distribution [35]. Because of that, we can conclude that the variations of S-W and cDB ratio curves are mainly due to changes in defect size and concentration. We have extended our investigations employing coincidence Doppler broadening (cDB) PAS [24] on ZnO and AZO films treated by FLA in N_2 atmosphere for 23 ms with a flash energy density of 66.4 J/cm^2, and the respective ratio curves, normalized to the ZnO single crystal reference and compared with Al defect-free bulk sample, are presented in Fig. 5c). Since cDB is highly sensitive to the high momentum electrons, hence core electrons, similarly as the W-parameter, but seems to be indifferent to Al substituting Zn sites, the observed changes of the ratio curves amplitudes reflect defect sizes, likely in the range of bi- or triple vacancy complexes, including zinc and oxygen vacancies [35]. Following the trend in ratio curves, the high momentum amplitude of the 1:40 case has a similar defect microstructure as the ZnO film, whereas decreasing the Zn content, larger vacancy agglomeration forms. At the same time, the 1:40 exhibits the lowest defect density, among all the other films, as the low electron momentum part $p_L < 5 \cdot 10^{-3}\ m_0c$ is the smallest, which is nicely reflected in the S-W plot, too (Fig. 5b)). According to the low-temperature PL by a 320 nm laser, the double peaks from near bandgap emission of AZO thin film proved that the Al atoms were incorporated with the ZnO lattices [11]. Additionally, from Fig. 3b), comparing the PL emissions from ZnO and AZO 1:20, Al-doped ZnO showed less optically-active-defect emissions.

3.3.2. *Variable energy positron annihilation lifetime spectroscopy*

In order to identify the type of defects created during the deposition process and the post-grown annealing, we have used Variable Energy Positron Annihilation Lifetime Spectroscopy (VE-PALS). The lifetime of positrons is a fingerprint of defect type and can be used to distinguish between different open volume sizes. In the case of monovacancies,

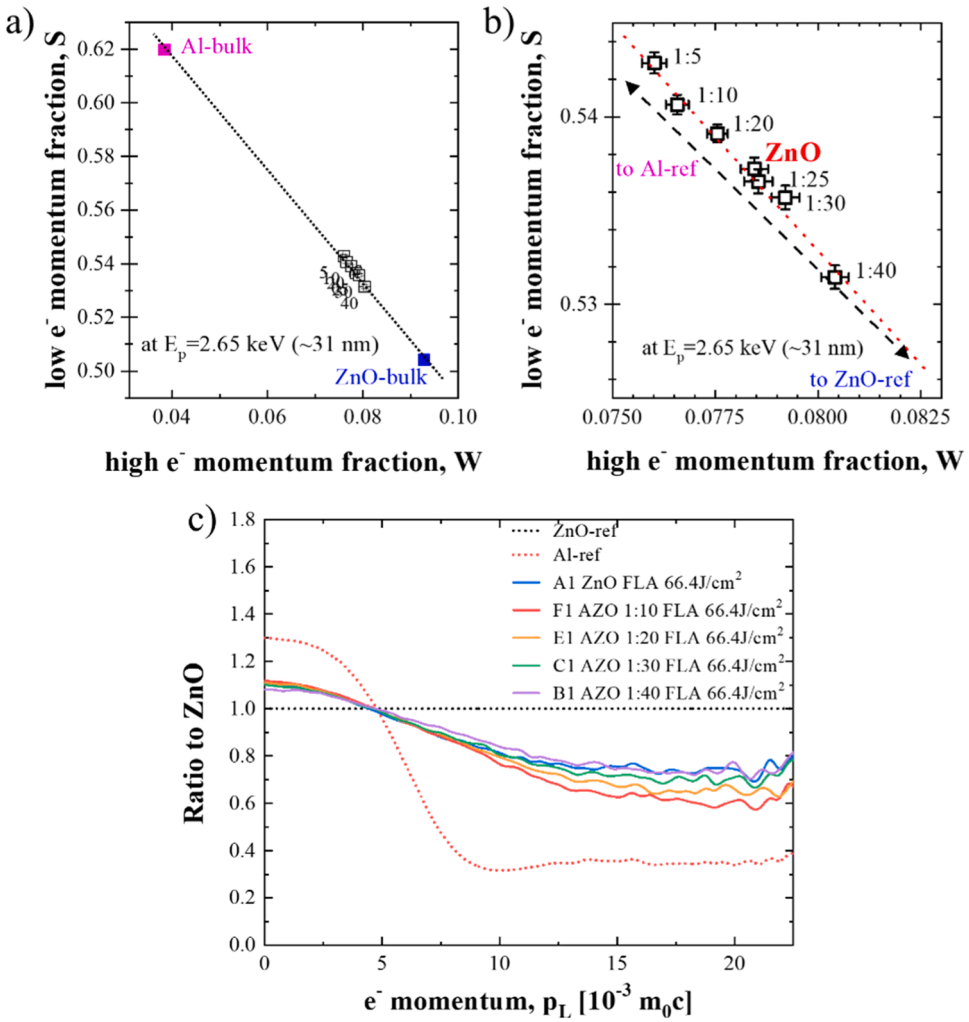

Fig. 5. a) The S-W parameters taken at about 31 nm from the surface of the films having different Al concentration treated by FLA in N_2 atmosphere for 23 ms with a flash energy density of 66.4 J/cm^2. b) Enlarged S-W plot, c) and coincidence Doppler broadening ratio curves of doped and undoped ZnO flashed with an energy density of 66.4 J/cm^2, normalized to a ZnO-reference crystal, indicating variation of defect sizes due to Al content.

positrons in ZnO can probe zinc vacancy (V_{Zn}) only, because oxygen monovacancy (V_O) is positively charged and not visible for positrons [35]. It is worth noticing that in a special case, the oxygen vacancies can be visualized by positrons if they form complexes with V_{Zn} or other defects. Moreover, positrons can annihilate in the defect-free ZnO as well. In such a case, the typical annihilation lifetime is in the range of 154 - 161 ps [36,37]. In our case, we did not detect such short lifetimes, most probably due to saturation of the annihilation process on the defective sites. Since our samples are heavily doped with Al and are nanocrystalline, the defect concentration is too high to measure the bulk annihilation lifetime.

Fig. 6a) shows the average positron annihilation time obtained from undoped ZnO before and after FLA. It can be seen that the average lifetime increases with increasing annealing temperature (flash energy density). It means that the average size of the open volume defects increases as well. Such a phenomenon is typically observed when small vacancies (mono- or divacancy) can diffuse and be trapped by larger defects, causing an increase of the average size of vacancy clusters or forming new vacancy clusters. The depth dependence of τ_{ave} exhibits a maximum close to the interface with the substrate, suggesting larger defects in that region. The maximum increases and shifts to lower depth with flash energy density as a consequence of raising open volumes. Fig. 6b) shows the spectrum deconvolution into positron lifetime components τ_1 and τ_2, which represent different defect sizes. The τ_1 corresponds to mono- and divacancies, and τ_2 is associated with vacancy clusters formed when more than several vacancies are bonded together. According to R. Magrin Maffei *et al.*, the positron annihilation lifetime of about 188 - 250 ps indicates the existence of small V_{Zn+nO} ($n < 4$) complexes, while the defect complex V_{nZn+O} ($n < 4$) has a lifetime range of 188–260 ps [35]. Since the obtained positron lifetimes were calculated from the unrelaxed structures, and the Boroński-Nieminen (BN) method [38] was used, the values are likely underestimated. Brauer *et al.* [39], proposed slightly larger positron lifetimes for V_{Zn} (229 ps) and V_{Zn+O} (276–286 ps) based on DFT ATSUP-BN calculations on optimized defect structures, which we highlight in Fig. 6b) for reference. The positron annihilation lifetime above 400 ps is typical for open volume defects made of 10 or more vacancies [40]. The depth distribution of intensity is presented in Fig. 6c). As can be seen with increasing annealing energy density, the intensity related to the shorter lifetime component decreases, while the second one increases, even though the lifetime changes mostly closer to the interface with the substrate. The change in the intensity confirms our assumption that the FLA process does not create new type of defects, but the concentration of defects changes. During FLA, the small defects diffuse and form small vacancy clusters due to the so-called Ostwald ripening process [41]. As a consequence of the Ostwald ripening process, the average number of point defects decreases, and big defects act as sinks for point defects.

Fig. 7a) shows the average positron lifetime obtained from as-grown

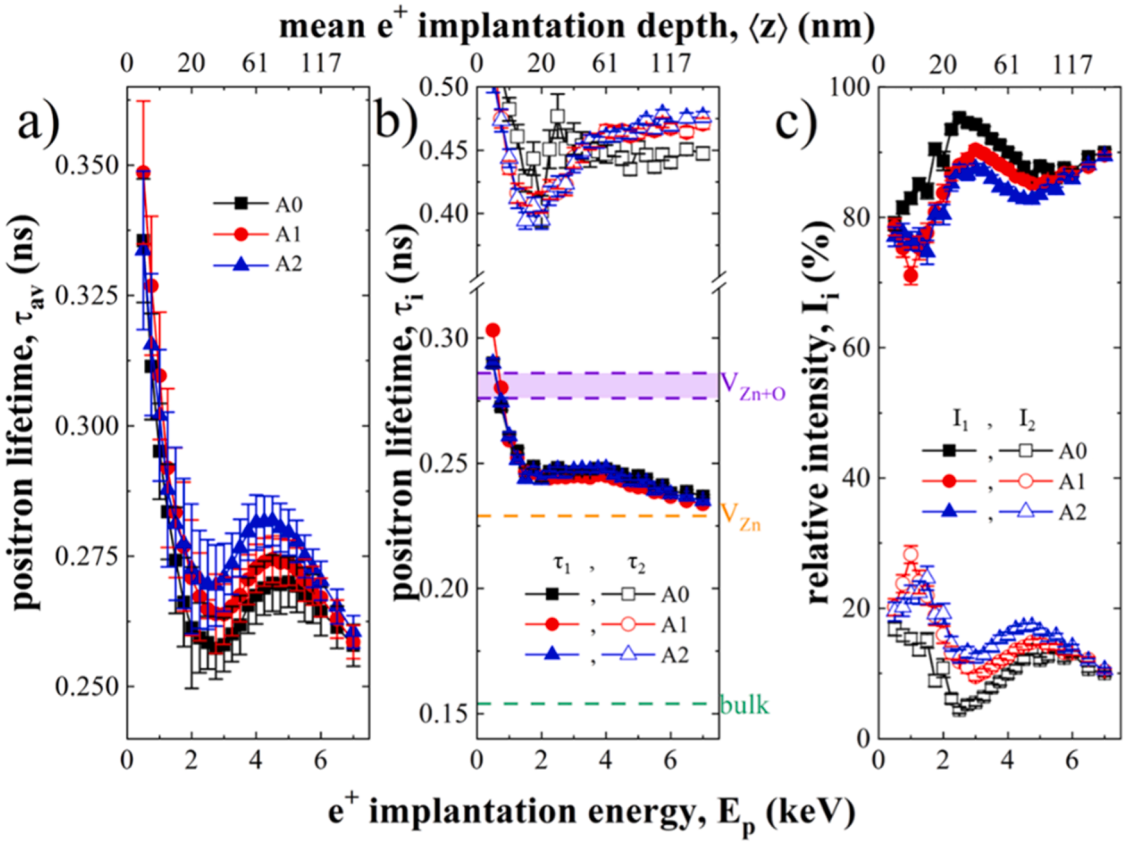

Fig. 6. a) Average positron lifetime of ZnO thin films before and after FLA, b) individual positron lifetime from different types of defects within ZnO thin films before and after FLA, and c) intensity of the lifetime for different samples. The intensity corresponds to the defect concentration. A0 is the as-deposited ZnO, A1 is ZnO flashed at an energy density of 66.4 J/cm^2, and A2 is ZnO flashed at 109.7 J/cm^2 by FLA, respectively.

AZO and annealed samples with a layer ratio between Al and Zn fixed at 1:20 i.e., the sample showing the highest electron concentration [11]. Compared to undoped ZnO, AZO samples are much more sensitive to the annealing conditions. In the middle of the layer, the τ_{av} increases from about 275 ps to 330 ps. Positron lifetimes τ_1 and τ_2 reveal that the FLA with the energy density of 66.4 J/cm^2 slightly affects the layer crystallinity, but after FLA at 107.4 J/cm^2 the average size of the vacancy cluster increases significantly (see Figs. 7b) and 7c)). Simultaneously, the concentration of small defects is reduced (lower intensity I_1), and the concentration of big clusters increases (I_2 increases). The dominant defect size in AZO films is larger compared to undoped ZnO films, as τ_1 is larger by about ~25 ps, hence closer to V_{Zn+O} than to V_{Zn}. Nevertheless, the dominant open volume defects detected by positrons are small V_{Zn}-based complexes and multi-vacancies at grain boundaries.

In this study, we employed various techniques to investigate the defects and microstructures of ZnO and Al-delta-doped ZnO (AZO) thin films. XRD and room-temperature PL results indicate that after flash-lamp annealing, the crystal quality of undoped ZnO and AZO films with lower Al concentrations improves. However, highly doped AZO films exhibited greater resistance to FLA and didn't present a significant change in XRD intensities. PL measurements further show the changes in emission before and after FLA. Specifically, for undoped ZnO, the red emission originating from defect levels shifts to green emission, indicating a transition in defect types from oxygen interstitials to zinc- or oxygen- vacancies. PAS and PALS provide insights into the defect types and concentrations within the thin films, both before and after FLA. In undoped ZnO, the dominant open volume defects are zinc vacancies (V_{Zn}), while in Al-doped ZnO, they are zinc and oxygen vacancy complexes (V_{Zn+O}). Due to the difference between measurement techniques and conditions, the conclusions drawn regarding defect concentrations from PL and PAS are not completely consistent, which indirectly indicates that non-radiative defect levels could exist in AZO-films.

4. Conclusion

In this work, we systematically investigated the influence of post-growth FLA on the microstructural and optical properties of undoped ZnO and δ-AZO thin films prepared by atomic layer deposition. The combined analyses of XRD, PL, TEM, and PAS provide a comprehensive understanding of the evolution of defects upon FLA treatment.

XRD results from the as-deposited samples confirm that the incorporation of a small amount of Al significantly improves the crystallinity of ZnO, whereas excessive Al doping suppresses this effect and increases the overall defect concentration. PL spectra reveal that FLA leads to a distinct change in optically active defect structure. TEM images further confirm that the designed superlattice structure of the delta-doped AZO films is preserved after FLA. PAS and PALS analyses identify zinc vacancies (V_{Zn}) as the primary open-volume defects in undoped ZnO, while zinc–oxygen vacancy complexes (V_{Zn+O}) dominate in Al-doped ZnO with an Al:Zn layer ratio of 1:20. The results also demonstrate that FLA for 23 ms promotes vacancy diffusion and defect reorganization through an Ostwald ripening process, in which smaller vacancies are trapped by larger ones, especially at grain boundaries.

Overall, this study reveals that moderate Al doping combined with optimized millisecond FLA is an effective strategy for achieving AZO thin films with improved crystallinity and enhanced conductivity. The insights gained from this work contribute to a deeper understanding of the defect dynamics in ZnO-based transparent conductive oxides and provide a practical guideline for defect engineering and performance optimization in future optoelectronic and sensor devices.

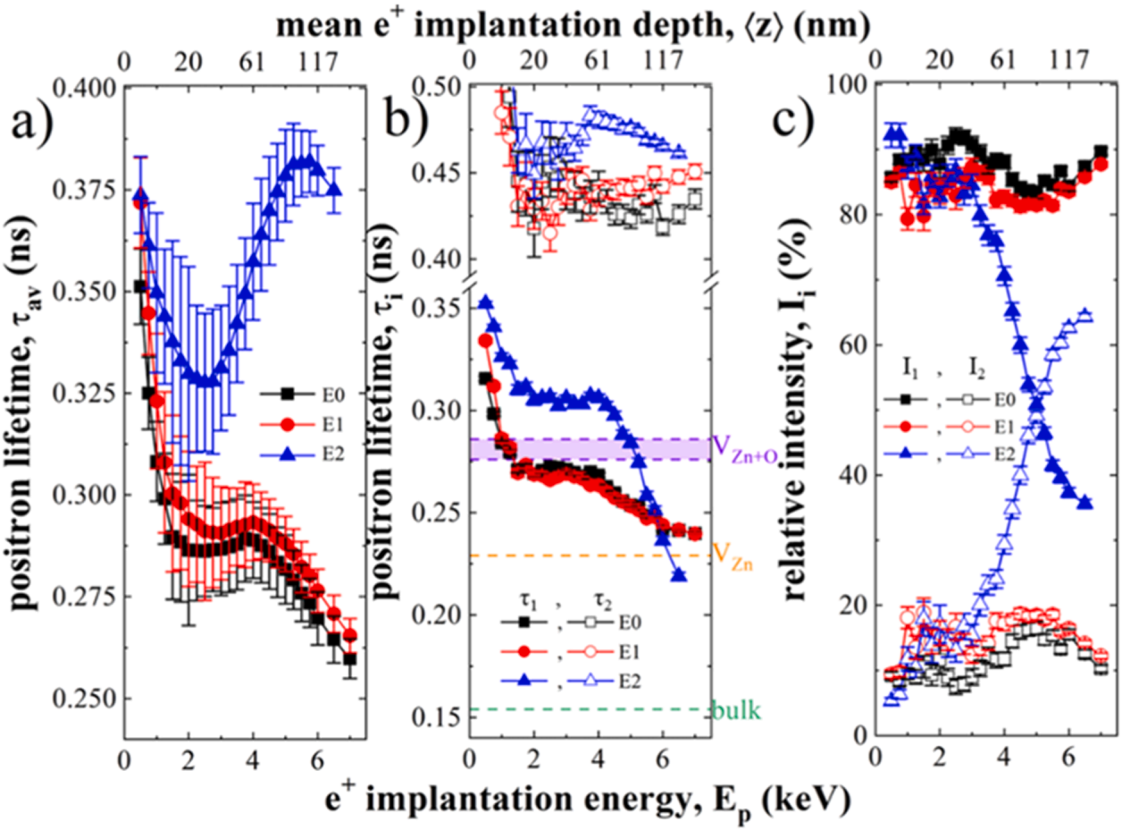

Fig. 7. a) Average positron lifetime of AZO 1:20 thin films before and after FLA, b) individual positron lifetime from different types of defects within AZO 1:20 thin films before and after FLA, and c) individual spectra intensity from different types of defects within AZO 1:20 thin films before and after FLA. E0 is the as-deposited AZO 1:20, E1 is flashed at an energy density of 66.4 J/cm^2, and E2 is flashed at 109.7 J/cm^2 by FLA, respectively.

Data availability

The data sets generated and/or analyzed during the current study are available from the corresponding author on reasonable request.

CRediT authorship contribution statement

Guoxiu Zhang: Writing – original draft, Validation, Investigation, Formal analysis. **Maciej Oskar Liedke:** Writing – review & editing, Validation, Formal analysis. **Maik Butterling:** Writing – review & editing, Validation. **Eric Hirschmann:** Writing – review & editing, Validation. **Andreas Wagner:** Writing – review & editing, Validation. **René Hübner:** Writing – review & editing, Validation. **Shengqiang Zhou:** Writing – review & editing, Supervision, Formal analysis. **Manfred Helm:** Writing – review & editing, Supervision. **Elizabeth von Hauff:** Writing – review & editing, Supervision, Formal analysis. **Slawomir Prucnal:** Writing – review & editing, Validation, Supervision, Formal analysis.

Declaration of competing interest

The authors declare that they have no known competing financial interests or personal relationships that could have appeared to influence the work reported in this paper.

Acknowledgement

The authors gratefully acknowledge the support by the Ion Beam Center (IBC), ELBE, and the Blitzlab at HZDR. We would like to thank the facility staff for their assistance. This work was partially supported by the Initiative and Networking Fund of the Helmholtz Association (FKZ VH-VI-442 Memriox) and the Helmholtz Energy Materials Characterization Platform (03ET7015). The authors thank Romy Aniol for TEM specimen preparation. The use of the HZDR Ion Beam Center TEM facilities and the funding of TEM Talos by the German Federal Ministry of Education and Research (BMBF, grant No. 03SF0451) in the framework of HEMCP are acknowledged.

Data availability

Data will be made available on request.

References

[1] J. Millan, et al., A survey of wide bandgap power semiconductor devices, IEEE Trans. Power Electron. 29 (5) (2013) 2155–2163.
[2] M.N. Yoder, Wide bandgap semiconductor materials and devices, IEEE Trans. Electron. Devi. 43 (10) (1996) 1633–1636.
[3] P.G. Neudeck, R.S. Okojie, L.-Y. Chen, High-temperature electronics-a role for wide bandgap semiconductors? Proceed. IEEE 90 (6) (2002) 1065–1076.
[4] T.P. Chow, R. Tyagi, Wide bandgap compound semiconductors for superior high-voltage power devices, in: [1993] Proceedings of the 5th International Symposium on Power Semiconductor Devices and ICs, IEEE, 1993.
[5] K. Tang, et al., Recent progress of the native defects and p-type doping of zinc oxide, Chin. Phys. B 26 (4) (2017) 047702.
[6] K. Ellmer, Past achievements and future challenges in the development of optically transparent electrodes, Nat. Photon. 6 (12) (2012) 809–817.
[7] P. Jongnavakit, et al., Surface and photocatalytic properties of ZnO thin film prepared by sol–gel method, Thin. Solid. Film. 520 (17) (2012) 5561–5567.
[8] K. Sun, et al., Preparation and performance of low-emissivity Al-doped ZnO films for energy-saving glass, Ceram. Int. 44 (16) (2018) 19597–19602.
[9] Y. Ammaih, et al., Structural, optical and electrical properties of ZnO: al thin films for optoelectronic applications, Opt. Quantum. Electron. 46 (2014) 229–234.
[10] S. Alamdari, M.J. Tafreshi, M.S. Ghamsari, Highly stable Ga-doped ZnO/polystyrene nanocomposite film with narrow-band cyan emission, J. Semiconduc. 43 (12) (2022) 122301.

[11] G. Zhang, et al., Al-delta-doped ZnO films made by atomic layer deposition and flash-lamp annealing for low-emissivity coating, Appl. Surf. Sci. 648 (2024) 159046.
[12] A.G. Attallah, et al., Millisecond flash lamp curing for porosity generation in thin films, Sci. Rep. 13 (1) (2023) 7765.
[13] J.B. Plumley, et al., Crystallization of electrically conductive visibly transparent ITO thin films by wavelength-range-specific pulsed Xe arc lamp annealing, J. Mater. Sci. 53 (18) (2018) 12949–12960.
[14] L. Rebohle, S. Prucnal, D. Reichel, Flash Lamp Annealing, 288, Springer, Switzerland, 2019, p. 15. Springer Series in Materials Science.
[15] H. Makino, et al., Influence of substrate temperature and Zn-precursors on atomic layer deposition of polycrystalline ZnO films on glass, Thin. Solid. Film. 517 (10) (2009) 3138–3142.
[16] M. Ramanachalam, et al., Characterization of ZnO varistor degradation using lifetime positron-annihilation spectroscopy, J. Appl. Phys. 69 (12) (1991) 8380–8386.
[17] A. Wagner, et al., Positron annihilation lifetime and doppler broadening spectroscopy at the ELBE facility, AIP Conf. Proc. 1970 (1) (2018) 040003.
[18] S. Prucnal, et al., Engineering of optical and electrical properties of ZnO by non-equilibrium thermal processing: the role of zinc interstitials and zinc vacancies, J. Appl. Phys. 122 (3) (2017) 035303.
[19] J. Lee, et al., Advancing Al-doped ZnO thin films structural, optical and electrical properties of low temperature PET substrates via flash lamp annealing, J. Semiconduct. 45 (12) (2024) 122101.
[20] M. Liedke, et al., Open volume defects and magnetic phase transition in Fe60Al40 transition metal aluminide, J. Appl. Phys. (16) (2015) 117.
[21] W. Anwand, et al., Design and construction of a slow positron beam for solid and surface investigations, Defec. Diffus. Forum. 331 (2012) 25–40.
[22] J. Dryzek, P. Horodek, GEANT4 simulation of slow positron beam implantation profiles, Nucle. Instrument. Method. Phys. Res. Sec. B 266 (18) (2008) 4000–4009.
[23] M. Clement, et al., Analysis of positron beam data by the combined use of the shape-and wing-parameters, J. Appl. Phys. 79 (12) (1996) 9029–9036.
[24] J. Cížek, Characterization of lattice defects in metallic materials by positron annihilation spectroscopy: a review, J. Mater. Sci. Tech. 34 (4) (2018) 577–598.
[25] E. Hirschmann, et al., A new system for real-time data acquisition and pulse parameterization for digital positron annihilation lifetime spectrometers with high repetition rates, J. Instrument. 16 (08) (2021) P08001.
[26] R. Krause-Rehberg, H.S. Leipner, Positron annihilation in semiconductors: defect studies. Solid-State Sciences, Springer, 1999.
[27] J.V. Olsen, et al., PALSfit: a new program for the evaluation of positron lifetime spectra, Phys. Status. Solid. C 4 (10) (2007) 4004–4006.
[28] M. Joseph, H. Tabata, T. Kawai, P-type electrical conduction in ZnO thin films by Ga and N codoping, JPN J. Appl. Phys. 38 (11A) (1999) L1205.
[29] T. Li, et al., Synthesis of highly-textured ZnO films on different substrates by hydrothermal route, Thin. Solid. Film. 518 (24) (2010) e114–e117.
[30] A.A. Al-Ghamdi, et al., Semiconducting properties of Al doped ZnO thin films, Spectrochim. Acta. Part A 131 (2014) 512–517.
[31] C. Koidis, et al., Growth mechanisms and thickness effect on the properties of Al-doped ZnO thin films grown on polymeric substrates, Phys. Status. Solid. 207 (7) (2010) 1581–1585.
[32] V. Kumar, et al., Origin of the red emission in zinc oxide nanophosphors, Mater. Lett. 101 (2013) 57–60.
[33] M.D. McCluskey, S. Jokela, Defects in zno, J. Appl. Phys. 106 (7) (2009).
[34] V. Gurylev, T.P. Perng, Defect engineering of ZnO: review on oxygen and zinc vacancies, J. Eur. Ceram. Soc. 41 (10) (2021) 4977–4996.
[35] R.M. Maffei, et al., Defectivity of Al: znO thin films with different crystalline order probed by Positron Annihilation spectroscopy, Appl. Surf. Sci. 665 (2024) 160240.
[36] S. Sharma, et al., Positron annihilation studies in ZnO nanoparticles, Solid. State. Commun. 149 (13–14) (2009) 550–554.
[37] Z. Chen, et al., Evolution of voids in Al+-implanted ZnO probed by a slow positron beam, Phys. Rev. B 69 (3) (2004) 035210.
[38] E. Boroński, R. Nieminen, Electron-positron density-functional theory, Phys. Rev. B 34 (6) (1986) 3820.
[39] G. Brauer, et al., Defects in virgin and N+-implanted ZnO single crystals studied by positron annihilation, hall effect, and deep-level transient spectroscopy, Phys. Rev. B—Condens. Matter. Mater. Phys. 74 (4) (2006) 045208.
[40] J. Cížek, et al., The development of vacancies during severe plastic deformation, Mater. Trans. 60 (8) (2019) 1533–1542.
[41] S. Tan, et al., Cluster coarsening in zinc oxide thin films by postgrowth annealing, J. Appl. Phys. 100 (3) (2006) 033502.